Flight Testing of Anti-windup Compensation in an Experimental UAV

Jorge Sofrony, Gary Balas and Matthew Turner

***Abstract*— Unlike most aircraft, truly autonomous UAV's have no "pilot" to monitor actuator position/rate saturation and to take action if either becomes too severe. Instead it is imperative that the control system itself features some mechanism of reacting to saturation and ensuring that the UAV remains stable and performance deterioration is minimal. This paper proposes the use of anti-windup techniques to fulfil this functionality and, in particular describes the application of modern anti-windup techniques to University of Minnesota's AEM-UAV testbed. Flight test results show that anti-windup compensation can significantly improve the performance of the UAV when rate-saturation of the ailerons is encountered. The results may be considered novel both because of the hitherto unreported application of anti-windup to UAV control and and because the results contribute to the bridging of the ever-growing gap between the theory and practice of anti-windup control.**

I. Introduction

Control magnitude and rate constraints are well-known in virtually areas of applied control and have become particularly notorious in the flight control community over the last several decades. They are one of the key factors in so-called Type 2 pilot-induced-oscillations (PIOs) which have been observed in the development of many highly augmented fly-by-wire aircraft[8]. At best, saturation of an aircraft's actuators causes some performance loss or ride discomfort, but the effects can be catastrophic as the crashes of the SAAB Grippen [1] and Boeing V22 Osprey aircraft [3] demonstrate.

Various methods of preventing or alleviating the effects of position, and often more importantly, rate limiting have been proposed in industry and in the literature. Of these, a particularly promising approach is that based on *anti-windup compensation* in which a (normally linear) baseline controller, which is known to function well in the absence of saturation, is augmented by another control element (the so-called anti-windup compenesator) which only becomes active once saturation occurs. The anti-windup compensator is present solely to assist the linear controller in maintaining stability and performance during periods of actuator saturation and should quickly de-activate after saturation has ceased. The advantage of such an approach is that the control system designer has full freedom in the design of the linear controller and, during normal operation, the system is unfettered by the anti-windup compensator. Recent applications of anti-windup to *manned* flight control applications are reported [4], [5], [13].

The focus of the flight control community, however, has drifted from manned aircraft to Unmanned Aerial Vehicles (UAV's), a field which has seen exponential growth in recent years due to the variety of military and civilian applications. Key to the future success of most UAV platforms is the need to improve reliability and reduce purchase and operating costs. In fact, most UAV accidents are due to system failures such as propulsion, data link and Flight Control Systems [**?**].

Not surprisingly, as with manned aircraft, actuator rate constraints in a UAV may lead to poor performance, or even cause instability, during aggressive or large amplitude manoeuvring. Although it may be possible to design the UAV control system in such a way that position/rate limits are not violated, such a strategy may lead to sluggish manoeuvrability, in effect sacrificing performance for robustness. In addition to the standard rate-limits, the servo-actuators used in UAV's are susceptible to degradation in their efficiency and thus the rate-limits may (unexpectedly) become more restrictive than initially designed; inducing further performance and stability problems. Some loss of efficiency failures have been modeled as rate-limits (see for example **??**) on the plant input, thus highlighting the fact that actuator rate constraints must be integrated into the flight control system design process to ensure higher levels of reliability. As noted above, unlike manned aircraft a UAV has no pilot on-board to monitor saturation effects and adjust flying strategy if necessary, and thus its control system must have sufficient capability to cope with saturation effects automatically.

The goal of this paper is to describe the application of modern anti-windup strategies, in which stability and performance guarantees during periods of saturation are given *a priori*, to a UAV problem. In particular, the paper describes the design and flight test of two anti-windup compensators the University of Minnesota's AEM-UAV testbed, and assesses the extent to which the compensators provide improved performance. The work presented follows similar structure to that presented in [5] and describes the design, implementation and flight-test of the anti-windup compensator, along with some tuning parameters that the designer must trade-off.

The paper structure is as follows: first the control problem to be addressed is described and the anti-windup compensation schemes adopted are briefly explained. Then the experimental setup is detailed and results from the flight tests are presented. The paper finalizes with some concluding remarks.

II. Problem Statement

The University of Minnesota's AEM-UAV experimental testbed, "Thor", is a low-cost experimental aircraft that allows a a streamlined validation process of controllers in a real flight environment. The focus of the paper is the roll axis control loop depicted in Figure II. The plant, $G(s)$, captures the lateral/directional dynamics of "Thor". Baseline control is provided by a PID controller driven by the roll attitude error and roll rate, with an added yaw damper driven by the yaw angle ψ (NOTE TO JORGE: IS THIS NOT "r" INSTEAD). The controller provides an aileron demand ζ to the actuators which then pass the rate-constrained signal $\hat{\theta}$ to the plant. The anti-windup compensator, $\Theta(s)$, is activated upon detection of aileron rate saturation and, when activated, modifies the baseline controller's behaviour in order retain stability and limit performance degradation. The baseline controller has been tuned in order to achieve desirable bank angle capture and fine tracking performance

under the assumption of no (or mild) rate saturation. It is assumed that rudder commands are not saturated and thus our attention will be solely focussed on the aileron constraints.

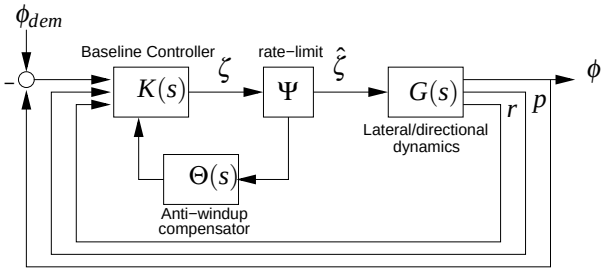

Fig. 1. Thor rate saturation compensation setup

A. Anti-windup interpretation

Under mild assumptions the scenario described above can be treated in a standard anti-windup framework [14]. First, it is assumed that the (dynamic) rate-limit nonlinearity $\Psi(.):\mathbb{R}\mapsto\mathbb{R}$ can be modelled as a first order feedback system involving a (static) saturation nonlinearity, viz

$$\Psi(s)\sim\left\{\begin{array}{rcl}\dot{x}_a &=& \mathrm{sat}(d)\\ \hat{\zeta} &=& x_a\\ d &=& H(\zeta-x_a)\end{array}\right. \tag{1}$$

This is a standard assumption in the literature - see [16], chapter 7 for example and a brief discussion. The plant represents the lateral/directional dynamics of "Thor" and is described by the finite dimensional linear time invariant model

$$G(s)\sim\left\{\begin{array}{rcl}\dot{x} &=& Ax+B\hat{\zeta}\\ y &=& Cx\end{array}\right.$$

where $y=[\phi\ p\ r]'$ is the measurement. The baseline linear controller can be represented as

$$K(s)=[K_r\ K_y]\sim\left\{\begin{array}{rcl}\dot{x}_c &=& A_cx_c+B_{cr}r+B_{cy}y\\ \zeta &=& C_cx_c+D_{cr}r+D_{cy}y\end{array}\right. \tag{2}$$

where $r=\phi_{dem}$. As the rate-limit is modelled by way of

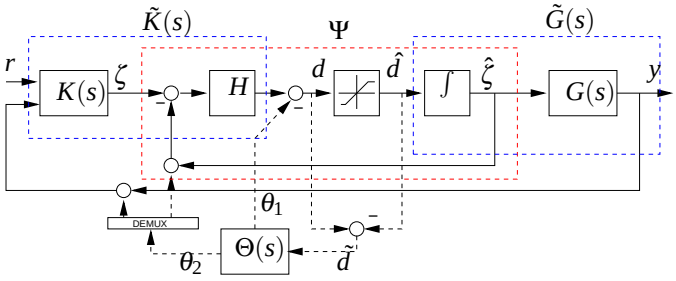

Fig. 2. Detailed schematic of anti-windup compensation and augmented plant and controller

a standard position limit, the anti-windup problem for rate-limits may then be manipulated in order to get a standard position-limit anti-windup problem. This is shown in Figure 2 where, in esssence, the rate-limit has been split so that part of it is absorbed into an augmented plant, $\tilde{G}(s)$ and part of it is absorbed into the controller in order to get an augmented controller, $\tilde{K}(s)$. The anti-windup compensator $\Theta(s)$ is driven by the signal $\tilde{d}=d-\hat{d}=\mathrm{Dz}(d)=d-\mathrm{sat}(d)$ and injects two signals into the closed loop, θ_1 and θ_2. Because the anti-windup compensator is driven by a "virtual" signal $d-\hat{d}$ a model of the rate-limits is normally included as part of the control algorithm. It then stands to reason that because the output of the model of the rate-limit is below the rate-limit thresholds, then the physical control signal will also have rates below the rate-limit threshold. The structure of the augmented plants and controllers therefore is

$$d=\underbrace{H\left[\begin{array}{ccc}K_r & K_y & -I\end{array}\right]}_{\tilde{K}}\left[\begin{array}{c}r\\ y\\ x_a\end{array}\right]\qquad\left[\begin{array}{c}y\\ x_a\end{array}\right]=\underbrace{\left[\begin{array}{c}G\frac{I}{s}\\ \frac{I}{s}\end{array}\right]}_{\tilde{G}}\mathrm{sat(d)} \tag{3}$$

It is noted that if no rate-saturation occurs, that is if $|d|<\bar{d}$ where $\bar{d}$ represents the aileron rate-limits, then the anti-windup compensator will not be active and the system will behave linearly with the performance and stability properties of the nominal linear system. Only when rate-saturation occurs will the anti-windup compensator become active.

B. Anti-windup design tools

Modern AW techniques have evolved greatly during the last decade and many AW synthesis techniques have been developed (see for example [16], [9] and references therein for example) using modern control tools. The main advantage of these modern tools over traditional approaches is that they are accompanied with performance and stability guarantees. Nonetheless, few of these techniques have been applied on "real" complex systems, and thus there is interest as to whether modern anti-windup schemes can perform well in practice. In this paper we follow the anti-windup design technique first introduced in [18] and in particular the design algorithms proposed in [17] and Chapter 5 of [15] (for example). These algorithms have been tested extensively in the (manned) SAIFE flight test campaign ([4], [7], [6]) for PIO resistance testing with much success and thus seemed a natural starting point for the work here.

For reasons which will become clear shortly, it is assumed that the anti-windup compensator is structured as

$$\Theta(s)=\left[\begin{array}{c}\Theta_1(s)\\ \Theta_2(s)\end{array}\right]=\left[\begin{array}{c}M(s)-I\\ \tilde{G}(s)M(s)\end{array}\right] \tag{4}$$

where $M(s)\in\mathscr{RH}_\infty$ represents some transfer function matrix yet to be specified. Using this particular anti-windup compensator structure, Figure 2 can be re-drawn as Figure 3 (see [14], [**?**] for further details). From Figure 3 note that the system exhibits a useful decoupling into nominal linear system, nonlinear loop and disturbance filter. Obviously the linear system exhibits desirable closed-loop behaviour so the task of the anti-windup compensator is to ensure (absolute) stability of the nonlinear loop and to ensure that the mapping from d_{lin} to $\tilde{y}_d=[y_d\quad x_{a,d}]$ is "small" in some sense. Note again that if d_{lin} does not exceed the saturation levels (i.e. rate-limiting does not occur), the upper part of the diagram is essentially redundant and linear behaviour continues inhindered.

The choice made for $M(s)$ effectively determines the type of anti-windup compensator used. The details are too lengthy for this paper, but it transpires that there are roughly two types of compensator which can be obtained: full order (FO) and low order (LO). FO compensators have order equal to

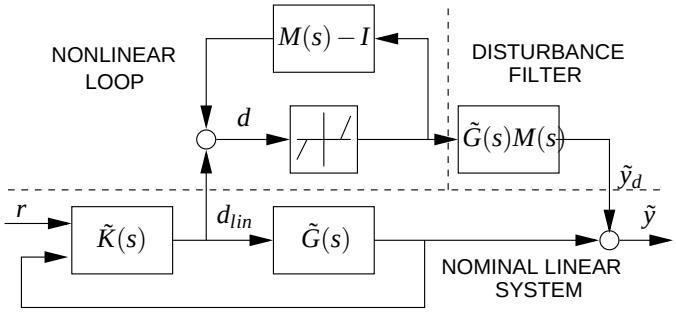

Fig. 3. Equivalent representation of Figure 2

that of the plant $\tilde{G}(s)$ and are *independent* of the linear controller. This makes them ideal for experimental systems where the main purpose is to validate control strategies rather than saturation resistance. However, because FO compensators tend to have high-order dynamics their effect on the closed-loop may linger some time after saturation has ceased, effectively leading to a slow recovery of linear behaviour.

LO anti-windup compensators have order less than the plant and allow the designer to have direct control over the compensator poles ([17], [2]), with an LMI-algorithm choosing "optimal" anti-windup gains. LO compensators may be preferred because the designer can elect not to include slow poles (notwithstanding stability requirements of course) so that the compensator's effect is removed from the loop soon after saturation has ceased. However LO compensators are designed using the nominal controller dynamics and thus lack the flexibility of the FO compensators. Despite this, it is often possible to get improved responses using LO compensators and it has been reported ([7], [2]) that AW schemes that depend on the controller may exhibit better performance in an AC system, thus enhancing even further handling qualities; this is in addition to computational advantages since it has a reduced number of states.

In this paper we will compare FO and LO AW compensation schemes where the compensators are designed are designed in a similar manner to those reported in [5] and **??**. In particular, assuming that the plant $\tilde{G}(s) \sim (A_p, B_p, C_p, 0)$, the following algorithms can be used to design anti-windup compensators.

Theorem 1 (Full-order AW compensation [15], Chapter 5): Given $\varepsilon \in (0,1)$ and assume that there exist matrices $Q = Q' > 0$, diagonal $U > 0$ and L, and scalar γ such that the following LMI condition is satisfied

$$\begin{bmatrix} A_pQ + QA_p' + B_pL + L'B_p' & B_pU - \varepsilon L & 0 & Q_pC \\ \star & -U & \varepsilon I & 0 \\ \star & \star & -\gamma I & 0 \\ \star & \star & \star & -\gamma I \end{bmatrix} < 0 \tag{5}$$

then there exists an anti-windup compensator $\Theta(s)$ such that the system in Figure 3 is globally asymptotically stable and that $\|\mathscr{T}_{d_{lin}}, \tilde{y}_d\|_{i,2} < \gamma$ for all $\mathrm{Dz}(.) \in \mathrm{Sector}[0, \varepsilon]$. Furthermore such a compensator can be constructed as

$$\Theta = \begin{bmatrix} M - I \\ GM \end{bmatrix} = \left[\begin{array}{c|c} A_p + B_pF & B_p \\ \hline F & 0 \\ C_p & 0 \end{array}\right] \tag{6}$$

where $F = LQ^{-1}$

Theorem 2 (Low-order AW compensation [17]): Given $\varepsilon \in (0,1)$ and (stable, low order) transfer functions $F_1(s)$ and $F_2(s)$, and assume there exists matrices $Q = Q' > 0$, diagonal $U > 0$, and L, and scalar γ such that the following LMI condition is satisfied

$$\begin{bmatrix} Q\bar{A}' + \bar{A}Q & B_oU + \bar{B}L - \varepsilon Q\bar{C}_1' & 0 & Q\bar{C}_2' \\ \star & -2U - 2\varepsilon UD_{01}' - 2\varepsilon L'\bar{D}_1' & \varepsilon I & UD_{02}'L'\bar{D}_2' \\ \star & \star & -\gamma I & 0 \\ \star & \star & \star & -\gamma I \end{bmatrix} < 0 \tag{7}$$

then there exists an anti-windup compensator $\Theta(s)$ such that the system in Figure 3 is globally asymptotically stable and that $\|\mathscr{T}_{d_{lin}}, \tilde{y}_d\|_{i,2} < \gamma$ for all $\mathrm{Dz}(.) \in \mathrm{Sector}[0, \varepsilon]$. Furthermore such a compensator can be constructed as

$$\Theta = \begin{bmatrix} F_1(s)\tilde{\theta}_1 \\ F_2(s)\tilde{\theta}_2 \end{bmatrix}$$

where $[\tilde{\theta}_1 \ \tilde{\theta}_2]' = LU^{-1}$, and the construction of matrices $\bar{A}$, B_o, $\bar{B}$, $\bar{C}_1$, $\bar{C}_2$, D_{01}, $\bar{D}_1$, D_{02}, $\bar{D}_2$ is detailed in [17]

Remark: The above theorems have been stated for $\mathrm{Dz}(.) \in \mathrm{Sector}[0, \varepsilon]$ where $\varepsilon \in (0,1)$, where as actuall $\mathrm{Dz}(.) \in \mathrm{Sector}[0,1]$. The reason for this is that because the augmented plant $\tilde{G}(s)$ incorporates the integrator dynamics from the rate-limit it is not asymptotically stable. It is well known in the anti-windup literature (for example [12], [11], [19], [16], [**?**]) that global internal stability and global finite $\mathscr{L}_2$ gain can only be obtained if the plant in question *is* asymptotically stable (or bounded real). To circumvent this difficulty we have thus used some "sector narrowing" techniques (see [10] for example) to approximate the sector in which the deadzone lies. In practice this means that our results are not *global* and if the control rate becomes too high (greater than $d/(1-\varepsilon)$) the anti-windup compensator may not function as expected. However, typically ε is small so the control system would have to be deeply saturated - which is unlikely in this application - before problems could be anticipated. We should also mention that there are techniques available to cope with other non-bounded real plants but we do not explore them here. □

III. Experimental Setup

A. Experimental Testbed

The AEM-UAV testbed "Thor" is a small radio controlled (RC) plane which has been modified to accommodate experimental control schemes, allowing the validation of different flight control system designs. The RC aircraft used is the *UltraStick 25E* (see figure 5) which is commercially available and has conventional horizontal/vertical dynamics with rudder and elevator control surfaces. The AC has symmetrical wing airfoil, where the longitudinal dynamics have aileron and flap control surfaces; flaps are not used in this experiment. Thor is a highly instrumented aircraft and features a customised avionics system which includes an IMU (Inertial Measurement Unit), GPS, pressure sensors and a pitot-tube. Propulsion is provided by a brushless DC motor connected to a propellar and standard servo-motors to actuate the control surfaces. The aircraft can be constantly monitored from a ground station and a ground safety pilot can override the flight computer and take command of the AC if he/she deems it necessary through a fail-safe system. When the AC is in autonomous flying mode, attitude and rate measurements of the roll and yaw angles are used for

feedback in the lateral/directional axis. The AC dynamics have been identified in [**?**] and describe a stable, well-behaved airframe. The main components of the experimental aircraft are depicted in Figure **??** and briefly described next.

Fig. 4. UltraStick 25E

Avionics: The complete avionic system, depicted in Figure **??**, consists of a flight computer and a suite of sensors that monitor system states and allow the implementation of experimental algorithms for guidance, navigation and control of the AC.

The *flight computer* is the phyCore MPC5200B-tiny development board which has a $32-bit$, $400Mhz$, PowerPC microprocessor. It can perform floating point operations and comes with a complete set of I/O ports that allow communication with external devices. Some of the supported protocols are RS-232, I^2C, SPI, and ethernet communication. The flight computer has a $64MB$ SDRAM memory that is used to store flight data which can later be downloaded via ethernet connection. The flight computer runs the *eCos* (embedded configurable operating system) real-time operating system and handles data collection from each sensor, performs attitude and position estimation , executes flight control algorithms, stores relevant data, outputs PWM servo commands, and sends information to the ground control station via the Maxstream, $900Mhz$, data modem [**?**].

The sensor architecture used is a combination of an IMU, a GPS, and a pitot-static system that allows an accurate measurement of the variables of interest. A low-cost integrated navigation system is difficult to find, thus the proposed architecture integrates individual sensors via estimation algorithms. Although this process may require more time to implement, it has the advantage of being flexible and easy to upgrade. The sensors used are described bellow:

- *IMU sensor*: The selected sensor is the ADIS16405 (Analog Devices). It is a small, low-cost, temperature compensated, tri-axial accelerometer, rate gyro, and magnetometer sensor unit which provides data to the flight computer via an SPI bus at $50Hz$.
- *GPS module*: The USGlobalSat EM-406A is compact and has an integrated antenna. It uses the SiRF StarIII GPS engine and data is provided to the flight computer via serial communication (RS-232) at $1Hz$.
- *Pressure sensors*: The AMSYS 5812 is a small solid-state, digital output, temperature-compensated pressure sensor. The sensor is connected to a pitot-static probe located forward on the right wing of the aircraft and is used to measure total and static pressure, thus determining airspeed and altitude of the aircraft. Pressure data is provided to the flight computer via I^2C bus at $50Hz$.

Actuators: All the control surfaces are actuated by standard *Hitec* analogue servomotors. The actuators of the control surface of interest (i.e. the aileron servomotors) have a bandwidth of $8Hz$ and rate limits of $2.6rad/sec$. The propulsion system consists of a $600W$ *E-Flite* electric brushless motor driving an APC 12×6 propeller and its ESC (electronic speed controller) that ensures rotational speed of the rotor.

Fail-safe System: Take-off and landing routines are performed by an RC pilot and, hence, it is necessary to switch to autonomous mode once take-off has concluded and the desired trim has been obtained, and then back to manual (piloted) mode when landing is required. The fail-safe system allows the pilot to regain command whenever he/she deems it unwise to fly autonomously.

Ground Control Station: The Ground Control Station is used to monitor the aircraft state and health status. It consists of a computer running software that connects, via a serial data modem, to the aircraft and retrieves information of interest. The GCS helps the pilot and designers to asses flight performance and monitor the development of the proposed task. The GCS software includes a heads-up display, a map showing the position of the aircraft, commanded command signals, and indicators that display flight mode information.

Fig. 5. Hardware Architecture

B. Test procedure

In order to test experimental designs, a test protocol must be followed to guarantee safety. The protocol consists of three steps: testing the algorithms on a full nonlinear model, testing the correct functioning of the software and on-board computer, and finally flight testing the real aircraft **??**. The steps are described next.

Software-in-loop: This stage consists of nonlinear simulations that run the controller code that will actually be embedded in the flight computer. This stage requires prototyping of the controller in $C-code$ and runs in a Matlab/Simulink environment. The main goal is to asses, via nonlinear simulation, the software code.

Processor-in-loop (PIL): This stage consists of simulation based hardware testing, and its main goal is to asses performance of the flight software and on-board computer before flight. The main setup consists of the flight computer running *in-the-loop* with the nonlinear UAV simulation; the Mathwork's Real-Time Windows Target toolbox is used to ensure the simulation runs in real time on a Windows PC. Flight dynamics and sensor data is simulated using the open source Flight Gear software, and fed to the flight computer which in turn runs the flight software; finally, correct PWM generation is tested. The PIL setup has a pilot interface via a USB-RC transmitter which enables all the functionalities available in a real flight setting, and aircraft state data can be monitored using the ground station software. If the the flight computer and software function properly, it is then possible to proceed to flight test.

Hardware-in-loop: This is the final stage where the controller is tested in a real flight environment. Flight test is executed in the following sequence: (i) first, the pilot performs a take-off task, climbing to approximately $86m$ in a straight and level manner; (ii) once trim is (approximately) achieved, the pilot switches to autonomous mode, where a pre-recorded set of reference commands, and control outputs, are executed taking no more than 15 seconds; (iii) finally, the pilot takes command and may either land the AC, or execute step (ii) once more.

IV. Experimental results

The effectiveness of AW compensation is demonstrated by considering a single up-and-away flight condition (FC). The tests were performed at FC $18.5m/s$ IAS, altitude $86m$ and involved the evaluation of two AW compensators, as described earlier. The tests focused on the roll axis exclusively, since it is desirable to maintain trim in order to reduce any uncertainty due to changes in FC. The AW compensators are therefore point-wise designs used to reduce the effects of rate limiting on the roll axis only. The evaluation reference signal was a (symmetric) pulse train with frequency $0.5Hz$, amplitude $0.38rad$ and duration 8 seconds. This signal proved to be of sufficient frequency and amplitude as to induced large deviations from linear closed-loop dynamics. In order to heighten the effects of rate saturation, software rate-limits were imposed on the aileron, where the limits were artificially degraded to 20% of the full authority values, i.e. the velocity of the ailerons is constraint to lay between $\pm 0.5rad/sec$.

A. Anti-windup design

The AW compensators designed were full and low order as discussed above. The design methods require the solution of a certain LMI, where the designer must choose key parameters which are the sector size (ε) for which stability and performance results hold, and the fixed compensator dynamics, $F_1(s)$ and $F_2(s)$, in the LO AW case. In addition to stability requirements of the compensator design, the transient response must be relatively fast as to swiftly recover linear dynamics once saturation periods have passed. The main parameters of the tested AW compensators are shown in table **??**.

Type	ε	Fixed Dynamics	Parameters	$\mathscr{L}_2$
FO	0.5	N/A	$F = \begin{bmatrix} -0.31 & 1.34 & 0.83 & \dots \\ 3.2 & 0 & -22.4 & \end{bmatrix}$	$\gamma = 0.5$
LO	0.5	$F_1(s) = \frac{40}{s+40}$ $F_2(s) = \frac{30}{s+30}$	$\tilde{\theta}_1 = [-2.03]$ $\tilde{\theta}_2 = [-0.0015,\ 0,\ 0.04]$	$\gamma = 1.5$

TABLE I
Compensator Parameters

Note that both compensators achieve a reasonably low upper bound on the $\mathscr{L}_2$ gain of the map $\mathscr{T}_{d_{lin},\tilde{y}_d}$ but that the low order design only has two states. Nonlinear simulations indicated that both compensators performed well for the references tested.

B. Flight test results

Flight tests were performed early in the morning in order to avoid (as much as possible) wind related perturbations. Four sets of flights were performed: two sets tested the no AW compensator case, while the two remaining sets tested the LO and FO AW compensators (one set per compensator). Each compensator was tested a total of five times per flight and an extra flight was performed for the full-authority (nominal rate limits) vehicle.

The results of the flight tests are presented in two ways: (i) time domain plots depicting tracking capabilities and aileron command signal, and (ii) RMS values of the tracking error and control action. In contrast to piloted missions where the control strategy is unknown, autonomous flight performance can be measured by using time domain data plots and RMS values. This is the case since the controllers gains are assumed to be constant throughout the mission and pilot perception does not apply to this problem setting.

Time Domain Plots

Time domain plots are useful in determining the system's gross aquisition and fine angle tracking capabilities in a qualitative manner. Figures 6 and 7 depict flight test data of the roll angle $(\phi(t))$ dynamics and aileron command signal after applying a predefined reference signal $\phi_{ref}(t)$.

Figure 6 shows the time response of the full-authority system, that is with no software rate limits are implemented. Observe that the nominal system has is well behaved with a settling time of approximately $0.4sec$ and good fine tracking properties (i.e. small steady state error). This response will be regarded as the "ideal" response, and performance of the AW compensators is assessed in against its deviation from this response. Note that the aileron command signal does not

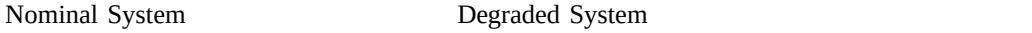

Fig. 7. Nominal and degraded RL closed-loop response

seem to be saturated in rate or position (nominal position saturation is $\pm 0.43[rad]$).

The left hand plots in Figure 7 show the degraded system response, with rate-limits of 20% of the AC's full authority values. Observe that roll attitude is out of phase with the roll attitude reference, and that large overshoots occur. This response is unacceptable as the roll angle reaches levels of up to $\pm 80[deg]$ and a considerable loss of altitude (loss of wing lift) was observed, thus operation of the AC under these conditions may be dangerous. Although reducing rate-limits to only 20% of their nominal value may seem extreme, this scenario is realistic in the RC community and must be addressed to enhance the reliability of low-cost UAV's. Note that the control signal appears to be rate-limited throughout the entire manoeuvre.

The use of rate-limit AW compensators may enhance system behavior during periods of velocity saturation, and can help the system retain nominal handling qualities. The middle and right plots of Figure 7 show the aircraft response with FO and LO anti-windup compensators engaged. In both cases the roll attitude is in phase with the reference and overshoot is dramatically reduced compared to the case when no AW is used. This demonstrates the improved system performance and stability margins during saturation periods, which can be obtained with anti-windup compensators.

As one of our objectives is to compare LO and FO closed-loop performance, observe how the LO compensator presents lower levels of overshoot, and thus exhibits better performance levels. The control effort and saturation level may also be of interest when analyzing performance of a compensator. Note that the LO order compensator seems to avoid the rate-limits and achieves a tracking performance close to the nominal, but with minimum control effort.

RMS values

As in [7], the RMS values of the tracking error and control action are used as another measure of closed-loop system performance. It is worth mentioning that the RMS tracking error values of the nominal system (Table II) are assumed to be optimal, hence AW compensated closed-loop systems may only aspire to reach similar level of tracking performance. When actuator degradation is implemented without AW complication, the RMS tracking errors approximately double, corroborating the observations from the time domain plots. Table III shows the RMS tracking errors obtained with AW engaged. While there is an increase in RMS tracking error observed with both LO and FO engaged (compared to the non-degraded system) these increases are much smaller than

Data set	Nominal		Degraded RL, noAW	
	RMS error	RMS command	RMS error	RMS command
Set 1	0.316	0.1292	0.7463	0.1263
Set 2	0.3186	0.1306	0.8027	0.1297
Set 3	0.3126	0.1269	0.7541	0.1278
Set 4	0.3337	0.1360	0.7893	0.1261
Set 5	0.329	0.1341	0.7488	0.1245

TABLE II
RMS ERROR AND CONTROL COMMAND VALUES FOR THE NOMINAL AND DEGRADED RATE-LIMITS WITH NO AW

Data set	Degraded RL, FO AW		Degraded RL, LO AW	
	RMS error	RMS command	RMS error	RMS command
Set 1	0.3872	0.0892	0.3572	0.0824
Set 2	0.3897	0.0910	0.3385	0.0788
Set 3	0.3900	0.0922	0.3520	0.0815
Set 4	0.4186	0.1022	0.3705	0.0875
Set 5	0.3944	0.0934	0.371	0.0864

TABLE III
RMS ERROR AND CONTROL COMMAND VALUES FOR THE DEGRADED RATE-LIMITS WITH FO AND LO AW ACTIVE

(a)

(b)

Fig. 6. Nominal system response: (a) reference roll angle command (dashed line) and AC roll position (solid line), (b) aileron command

without AW. The increases in RMS error for the LO compensator are lower than the FO compensator, again indicating its superiority perhaps due to reduced order dynamics and account of controller dynamics in design.

V. CONCLUSIONS

This paper has presented the flight test evaluation of two types of AW compensator on the University of Minnesota's UAV testbed. As in previous results reported in [5], [6] for the piloted case, flight test data supports the fact that AW compensation provides noticeable system performance enhancement during periods of rate-saturation, and is well suited for aerospace applications. The LO order compensator appeared to perform particularly well which, together with its simple implementation, perhaps make it the preferred AW strategy. Nevertheless the FO should not be discounted since in some experimental systems the controller may frequently be replaced and so a controller-independent system such as the FO compensators may be preferable. The price is paid is a higher computational burden and lower, but still acceptable, performance enhancement.

The crucial difference in the *manned* and *unmanned* applications is that in unmanned applications there will typically no pilot to adjust reference demands etc when rate-saturation occurs in order to keep the system operating linearly. Instead, some automatic system must be able to monitor saturation levels and act accordingly to preserve stability and performance when saturation is encountered. Anti-windup seems to be a promising candidate for this task.

Finally, it is important to mention that AW compensation may be regarded as a fault-tolerant control (FTC) control scheme where the controller suffers reconfiguration once degraded levels of efficiency are detected in the actuators. This, and other types of actuator faults may be modeled as nonlinear static function that may be *neutralized* by using AW based strategies.

REFERENCES

[1] Anon. Why the grippen crashed. *Aerospace America*, page 11, 1994.

[2] J.-M. Biannic and S. Tarbouriech. Optimisation and implementation of dynamic anti-windup compensators with multiple saturations in flight control systems. *Control Engineering Practice*, 17(6):703–717, 2009.

[3] C. Bolkcom. V-22 osprey tilt-rotor aircraft. *CRS Report for Congress*, page Code RL31384, 2005.

[4] O. Brieger, M. Kerr, D. Leissling, I. Postlethwaite, J. Sofrony, and M.C. Turner. Anti-windup compensation of rate saturation in an experimental aircraft. In *Proc. American Cont. Conf.*, New York, 2007.

[5] O. Brieger, M. Kerr, D. Leissling, I. Postlethwaite, J. Sofrony, and M.C. Turner. Flight testing of a rate saturation compensation scheme on the attas aircraft. *Aerospace Science and Technology*, 13(2-3):92–104, 2009.

[6] O. Brieger, M. Kerr, D. Leissling, I. Postlethwaite, J. Sofrony, and M.C. Turner. Pilot-involved-oscillation suppression using low-orderanti-windup: Flight test evaluation. *Journal of Guidance, Control, and Dynamics*, (To Appear), 2012.

[7] O. Brieger, M. Kerr, I. Postlethwaite, J. Sofrony, and M.C. Turner. Flight testing of low-order anti-windup compensators for improved handling and pio suppression. In *Proc. American Cont. Conf.*, Seattle, 2008.
[8] H. Duda. Prediction of pilot-int-the-loop osciallations due to rate saturation. *Journal of Guidance, Control and Dynamics*, 20(3):581–587, 1997.
[9] S. Galeani, S. Tarbouriech, M.C. Turner, and L. Zaccarian. A tutorial on modern anti-windup design. *European Journal of Control*, 15(3-4):418–440, 2009.
[10] H. Hindi and S. Boyd. Analysis of linear systems with saturation using convex optimization. In *37th IEEE Conference on Decision and Control*, pages 903–908, Tampa, Florida, USA, 1998.
[11] J.M. Gomes da Silva Jr., S. Tarbouriech, and G. Garcia. Local stabilization of linear systems under amplitude and rate saturating actuators. 48(5):842–847, 2003.
[12] M.V. Kothare, P.J. Campo, M. Morari, and C.N. Nett. A unified framework for the study of anti-windup designs. *Automatica*, 30(12):1869–1883, 1994.
[13] L. Rundqwist and R. Hillgren. Phase compensation of rate limiters in jas 39 gripen. *AIAA-96-3368-CP*, 1996.
[14] J. Sofrony, M.C. Turner, I. Postlethwaite, O.M. Brieger, and D. Leissling. Anti-windup synthesis for PIO aviodance in an experimental aircraft. *IEEE Conference on Decision and Control*, 2006.
[15] S. Tarbouriech, G. Garcia, and A.H. Glattfelder. *Advanced Strategies in Control Systems with input and Output Constraints*. Springer-Verlag, London, 2006.
[16] S. Tarbouriech, G. Garcia, J.M. Gomes da Silva, and I. Queinnec. *Stability and stabilisation of linear systems with actuator saturation*. Springer, London, 2011.
[17] M.C. Turner and I. Postlethwaite. A new perspective on static and low order anti-windup synthesis. *International Journal of Control*, 77(1):27–44, 2004.
[18] P.F. Weston and I Postlethwaite. Linear conditioning for systems containing saturating actuators. *Automatica*, 36(9):1347–1354, 2000.
[19] F. Wu and B. Lu. Anti-windup control design for exponentially unstable lti systems with actuator saturation. *Systems and Control Letters*, 52:305–322, 2004.